Determination of the Electronic Energetics of CdTe Nanoparticle Assemblies on Au Electrodes by Photoemission, Electrochemical, and Photocurrent Studies

ARTICLE *in* THE JOURNAL OF PHYSICAL CHEMISTRY C · AUGUST 2012

Impact Factor: 4.77 · DOI: 10.1021/jp306702t

9 AUTHORS, INCLUDING:

Zuoti Xie
University of Minnesota Twin Cities
15 PUBLICATIONS **209** CITATIONS
SEE PROFILE

Ron Naaman
Weizmann Institute of Science
304 PUBLICATIONS **5,449** CITATIONS
SEE PROFILE

THE JOURNAL OF PHYSICAL CHEMISTRY C

Article

pubs.acs.org/JPCC

Determination of the Electronic Energetics of CdTe Nanoparticle Assemblies on Au Electrodes by Photoemission, Electrochemical, and Photocurrent Studies

Yang Wang,[†,⊥] Zuoti Xie,[‡,⊥] Gilad Gotesman,[‡] Lei Wang,[†] Brian P. Bloom,[†] Tal Z. Markus,[‡] Dan Oron,[§] Ron Naaman,[‡,*] and David H. Waldeck*[,†]

[†]Department of Chemistry, University of Pittsburgh, Pittsburgh, Pennsylvania 15260, United States

[‡]Department of Chemical Physics, [§]Department of Physics of Complex Systems, Weizmann Institute of Science, Rehovot 76100, Israel

Supporting Information

ABSTRACT: This work explores the electronic states of CdTe semiconductor nanoparticles (NPs) that are immobilized on a polycrystalline Au film through an organic linker (dithiol). The HOMO and LUMO energies of the CdTe NPs were determined by using photoelectron spectroscopy and cyclic voltammetry. The results from these measurements show that the HOMO energy is independent of the nanoparticle size and is pinned to the Fermi level, whereas the LUMO energy changes systematically with the size of the NP. Studies with different capping ligands imply that the dithiol ligand removes surface states and enhances the optoelectronic properties of the NPs.

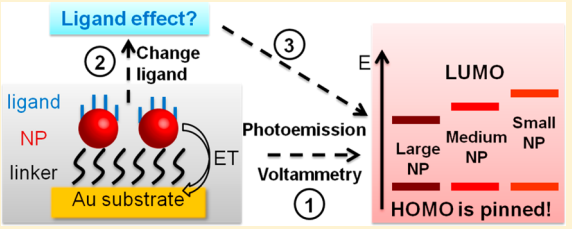

1. INTRODUCTION

The electronic structure of semiconductor nanoparticles (NPs) is important for their use in optoelectronics,[1] photovoltaics,[2−4] and photocatalysis.[5] In order to optimize performance of the NP in these applications, it is necessary to understand and control the alignment between the energy levels of the NPs and the substrates (or electrodes), e.g., at the interface of NPs and a TiO_2 substrate in a quantum dot sensitized solar cell,[6] or at the interface of NPs and a back metal contact in a Schottky photovoltaic device.[7] Although much is known from the solid-state physics literature about semiconductor and metal−semiconductor interfaces, relatively few works have addressed the metal−semiconductor nanoparticle interface. This work uses photoelectron spectroscopy and electrochemistry methods to probe the electronic states of CdTe NPs that are assembled into a monolayer film on a polycrystalline Au film by a dithiol (DT) linker.

In an earlier study, we used photoelectron spectroscopy (PES) and cyclic voltammetry to investigate the electronic states of CdSe NPs that were adsorbed on a polycrystalline Au film via a DT organic linker.[8] That study showed that the HOMO energy of the CdSe NP was independent of its size (for sizes greater than 2.8 nm diameter), and it was pinned at ∼1.25 eV below the Fermi level of the Au. In contrast, the LUMO energy of the CdSe NP changed systematically with its size. A similar effect was reported by us for the case of CdSe/ZnS core/shell NPs.[9] Also, in the case of CdSe[10] and PbSe[11] NPs, it has been reported that the HOMO is 'pinned' to the Fermi level of a ZnO semiconductor substrate, when a short organic linker, such as 3-mercaptopropionic acid or ethanedithiol, is used to tether them. Presumably, the pinning results from a high density of interfacial states at the metal−nanoparticle interface.[8,12]

Given these reports for the Fermi level pinning of CdSe NPs and the chemical similarities of CdSe and CdTe, it is interesting to explore the nature of the CdTe NP interaction with Au and whether the HOMO of CdTe NPs is pinned relative to the Fermi level of Au. Two earlier studies have examined the electronic states of CdTe NPs at electrode interfaces. Haram et al.[13] used cyclic voltammetry to determine the HOMO and LUMO energies of CdTe NPs diffusing in solution. Under these conditions, the electrochemical and optical determinations of the HOMO−LUMO gap were in excellent agreement, and they found that the HOMO energy changed with the size of the NP—presumably because it was not immobilized on the electrode. Jasieniak et al.[14] used a photoelectron spectroscopy in air method to examine the electronic states of CdSe and CdTe NPs in drop cast films on indium−tin oxide electrodes. Their data suggest a weak dependence of the HOMO energy on the particle size for both CdSe and CdTe NPs. The HOMO and LUMO energies that were assigned to the CdTe NPs in these two studies differ by 0.5−1.0 eV. Part of this energy difference may be caused by the different capping ligands on the NPs used in those two works; it has been reported that the dipole moment of the ligand can affect the energetics of the NPs.[15] Another complicating feature of the comparison is the

Received: July 6, 2012
Published: August 1, 2012

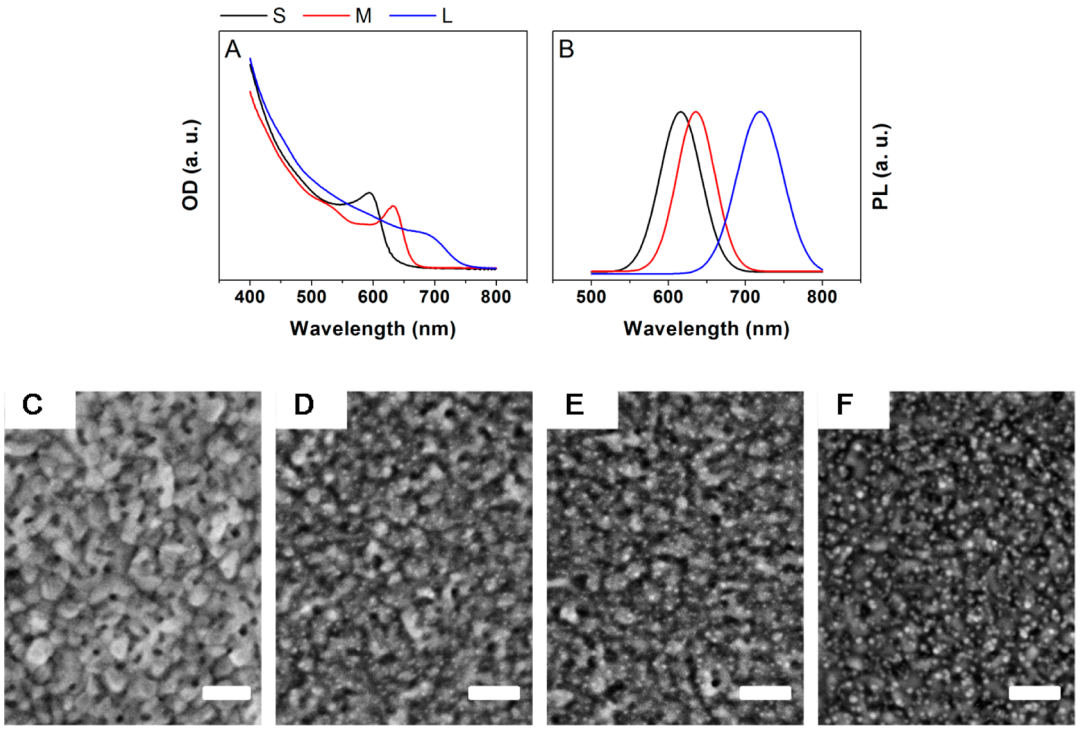

Figure 1. (A and B) Steady-state absorption (OD) and photoluminescence (PL) spectra, respectively, for the small (S, black), medium (M, red), and large (L, blue) CdTe NPs in toluene. (C–F) SEM images, respectively, for the bare Au substrate (C), Au/DT/S-NP (D), Au/DT/M-NP (E), and Au/DT/L-NP (F). All scale bars are 100 nm.

different substrate/electrode that was used in these two studies.[11]

This work examines the electronic states of CdTe NPs on Au electrodes by photoemission and cyclic voltammetry. The same substrate, the same capping ligand, and the same sample preparation method are used for the photoelectron spectroscopy and cyclic voltammetry measurements to ensure that the two systems are quantitatively comparable. This work provides a rigorous determination of the HOMO and LUMO energies of CdTe NPs and demonstrates consistency between the photoemission and cyclic voltammetry methods. This study finds that the HOMO of the CdTe NPs is pinned with respect to the Fermi level and that the capping ligands affect the exciton lifetime of the CdTe NPs.

2. EXPERIMENTAL METHODS AND MATERIALS

2.1. Materials. Cadmium oxide and trioctyl phosphine (TOP) were purchased from Strem Chemicals. Tetradecylphosphonic acid (TDPA) was purchased from PolyCarbon Industries. All of the other chemicals were purchased from Sigma Aldrich and were used without further purification, unless mentioned otherwise.

2.2. Synthesis of NPs. TDPA-CdTe nanoparticles (NPs) were synthesized by using previously published methods.[16] Briefly, a solution of the tellurium precursor (0.2 mmol Te/1 mL TOP) was hot-injected into a solution of the cadmium precursor (0.4 mmol CdO/0.8 mmol TDPA/5 mL 1-octadecene) at 300 °C. The sizes of the NPs were controlled by the duration of the reaction and by extra injections of the cadmium and tellurium precursors. Panels A and B of Figure 1 respectively show the steady-state absorption and photoluminescence spectra measured in toluene for the small (S), medium (M), and large (L) CdTe NPs used in this work. By inputting the wavelength of the first excitonic peak into an established model,[17] the average size of the NPs is calculated to be about 3.71 nm for S, 4.15 nm for M, and 6.00 nm for L NPs.

2.3. Sample Preparation. The Au substrate was either 150 nm thick Au films on silicon (100) for photoelectron spectroscopic measurements, or it was Au ball electrodes for cyclic voltammetry and photocurrent measurements in an electrochemical cell. The same procedure was used to make NP assemblies in both cases. Namely, the clean Au substrate was immersed overnight in a methanol solution of 1 mM 1,9-nonanedithiol (DT) to create a monolayer of DT on the Au surface. The Au–dithiol substrate (Au/DT) was then placed into a toluene solution of CdTe NPs (optical density around 0.2) for 0.5–3 h to immobilize the NPs on the surface, creating a Au/DT/NP assembly. This assembly process was characterized by scanning electron microscopy (SEM). Panels C–F of Figure 1 respectively show SEM images for the bare Au substrate, the small NPs on Au (Au/DT/S-NP), the medium NPs on Au (Au/DT/M-NP), and the large NPs on Au (Au/DT/L-NP). These images reveal the roughness features of the evaporated Au film and illustrate that different NP sizes are adsorbed onto the Au/DT substrate in the three cases. Based on the SEM images, the surface coverage of the NPs on Au is estimated to be about 750/μm^2 for the S-NPs, 1250/μm^2 for the M-NPs, and 2500/μm^2 for the L-NPs.

For studies requiring a capping layer of DT on the CdTe NPs, the Au/DT/NP assemblies were immersed into the DT solution again to create an assembly of Au/DT/NP/DT.

2.4. Photoelectron Spectroscopy. Both single-photon and two-photon photoelectron techniques were used to determine the band edge energies of CdTe NPs. The Au/DT/NP assemblies were placed in an ultrahigh vacuum chamber ($<10^{-8}$ Torr) where an incident laser pulse excited the samples, and the energy of the photoelectron was measured by a time-of-flight spectrometer. More details of the apparatus

dx.doi.org/10.1021/jp306702t | J. Phys. Chem. C 2012, 116, 17464–17472

can be found in reference 18. Because the Au substrate is grounded and the laser intensity and repetition rate (10 Hz) are kept low, the samples do not retain any significant amount of net charge between laser pulses. This was verified by observing a stable electron energy spectrum which does not vary with time.

For the single-photon low-energy photoelectron transmission spectroscopy (LEPET, Scheme 1A), the photon energy is higher than the work function of the sample, so that the photoelectrons are directly ejected from states below the Fermi level to above the vacuum level and transmitted to the detector. This measurement provides information on the sample's density of states below the Fermi level, including the HOMO of the NP and surface states of the substrate and the NPs.[18]

The two-photon photoelectron spectroscopy method (TPPE, Scheme 1B) uses photons with an energy lower than the work function of the sample. The first photon, the "pump" photon, excites electrons from below the Fermi level to unoccupied states (i.e., the "intermediate" states) above the Fermi level but below the vacuum level. Although most of the electrons relax fully to the Fermi level, some fraction is captured by the lowest unoccupied state (the LUMO) of the nanoparticle where they can be trapped for a longer time. If a second laser photon (the 'probe' photon) arrives on the sample before all of the trapped electrons recombine back into the metal substrate, then some fraction of these electrons can be excited to above the vacuum level. Thus, the measured kinetic energy of these photoelectrons provides information about the energy of the metastable state, LUMO of the NPs.

Scheme 1. Schematic Description of the Photoelectron Spectroscopic Techniques Used in This Study; (A) Low-Energy Photoelectron Transmission Spectroscopy (LEPET) for Measuring the HOMO; (B) Two-Photon Photoelectron Spectroscopy (TPPE) for Measuring the LUMO

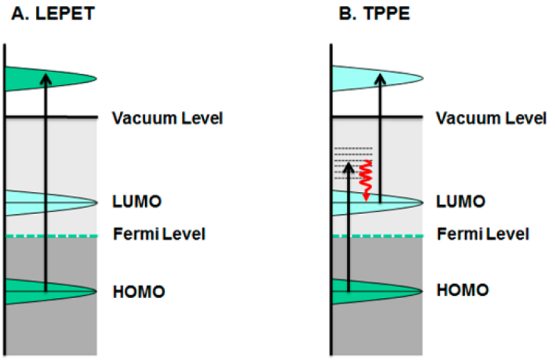

2.5. Cyclic Voltammetry. The cyclic voltammetry was performed in a three electrode electrochemical cell with a CHI 618B potentiostat. A chemically modified Au ball electrode (e.g., Au/DT/NP) was used as a working electrode, a Pt wire was used as a counter electrode, and $Ag/AgNO_3$ was used as a reference electrode (0.1 V vs Fc/Fc^+). The supporting electrolyte was a 100 mM acetonitrile solution of tetrabutylammoniumhexafluorophosphate ($TBAPF_6$). The scan rate was 0.05 V/s.

2.6. Photocurrent Measurement. Photocurrent measurements at a controlled bias potential were performed in the same electrochemical cell. In these studies triethanolamine (TEA) was added into the supporting electrolyte solution at a concentration of 20 mM to act as a hole scavenger and ensure a stable photocurrent. The illumination was provided by a 75 W Xe arc lamp coupled with a multimode optical fiber. At a working distance of 2.54 cm, this setup provided an illumination area of 7 mm^2. The illumination was chopped at 1 Hz by a motorized shutter. See reference 3 for more details.

3. RESULTS

3.1. Photoemission Studies. *3.1.1. LEPET.* Figure 2A shows LEPET spectra for the dithiol-coated gold electrodes (Au/DT) and three different gold/dithiol/nanoparticle (Au/DT/NP) assemblies when excited by 6.42 eV photons. Because the LEPET method measures the density of states below the Fermi level, the high kinetic energy cutoff (3.05 ± 0.05 eV) corresponds to the photoelectrons ejected from just below the Fermi level. For the Au/DT reference substrate, the work function is Φ = 4.6 ± 0.1 eV (given by the photon energy minus the total width of the spectrum, ~1.8 eV). The Au/DT/NP assemblies (Φ = 4.2 ± 0.1 eV) exhibited a strong peak at a kinetic energy of about 1.3 eV, which is not present in the Au/DT reference sample. The photoelectron signal of this peak increases as the surface coverage of the NP increases (see Figure S1 in Supporting Information). Thus, the peak at 1.3 eV is assigned to photoelectrons ejected from the filled levels of the NPs. Figure 2B shows the photoelectron signal of the Au/DT/NP assemblies after the signal from the Au/DT reference has been subtracted, and Figure 2C shows a plot in which the resultant spectra are rescaled to the same peak height. Using the rescaled spectra in Figure 2C, the HOMO (or band edge) energy of the NP was determined by linearly extrapolating on

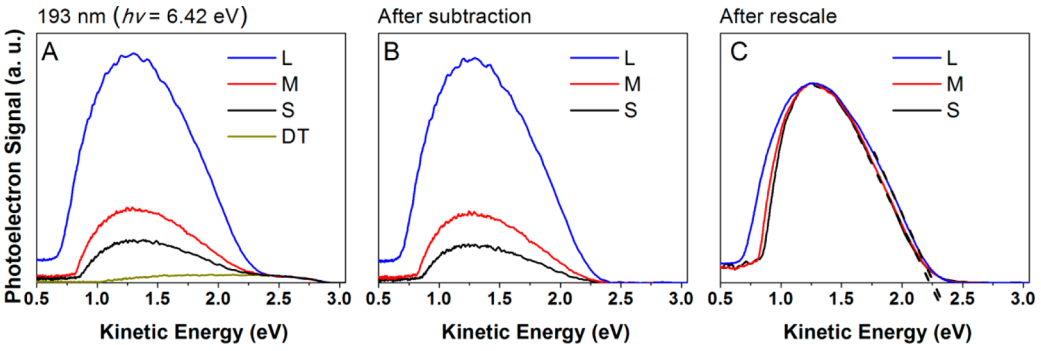

Figure 2. (A) LEPET spectrum for Au/DT (dark yellow), Au/DT/S-NP (black), Au/DT/M-NP (red), and Au/DT/L-NP (blue). L, M, and S indicate the nanoparticle size: large, medium, and small, respectively. (B) Corresponding spectra after the subtraction of the Au/DT spectrum. (C) Spectra in panel B after scaling them to the same signal height and the extrapolation to the high kinetic energy cutoff.

dx.doi.org/10.1021/jp306702t | J. Phys. Chem. C 2012, 116, 17464–17472

the high kinetic energy side to determine a cutoff energy. For all three sizes of NPs, the photoelectron distribution has the same cutoff kinetic energy of 2.25 ± 0.05 eV. This value is 0.80 ± 0.05 eV below the Au/DT Fermi level and is assigned to the HOMO energy of the CdTe NPs. In A and B of Figure 2, the size-dependent variations in the spectral intensity and width are likely caused by the difference in the NP surface coverage on Au and/or the NP absorption cross section.

The LEPET data in Figure 2 demonstrate that the HOMO energy of the CdTe NPs does not change over the NP size range of 3.7 to 6.0 nm. Although differing in details, these data are similar to that reported earlier for CdSe NPs immobilized on Au electrodes.[8,9] A quantitative comparison with the previous CdSe NP result shows that the HOMO energy of CdTe NPs assembled on Au/DT is about 0.4 ± 0.1 eV higher than that of CdSe NPs. This difference is similar to that reported by Jasiniek[14] for drop cast films of CdSe NPs and CdTe NPs on ITO.

3.1.2. TPPE. Because the HOMO/LUMO bandgap changes with the NP size and the HOMO energy is not changing with the NP size, one expects that the LUMO energy should shift with the size of the NPs.[8] Unfortunately, the TPPE spectra (see Figure S2 in Supporting Information [SI]) for the assemblies of Au/DT/NP do not show a clear signal from the LUMO of the NP. This result suggests that the excited electron on the LUMO level recombines too rapidly for a sufficient population of metastable electrons to be created. Attempts to increase the population by increasing the laser intensity were not successful because of the onset of direct nonlinear photoemission. In order to increase the population of trapped electrons in the nanoparticle's LUMO, the organic capping ligand was exchanged in order to change the surface state distribution on the NP and decrease the surface recombination rate.[19,20] Because thiol ligands are known to extend the exciton lifetime for the CdTe NPs,[19] a second monolayer of dithiol (DT) molecules was used to replace the TDPA from the immobilized NPs (Scheme 2).

Scheme 2. Ligand Exchange Process from Au/DT/NP to Au/DT/NP/DT

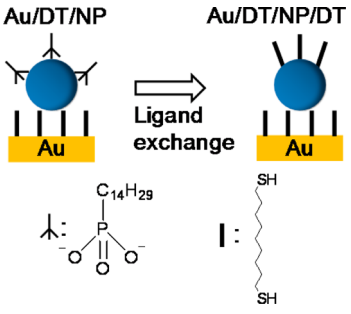

After replacing the TDPA ligand with a thiol ligand, the TPPE spectra showed a clear spectral signature from metastable electronic states. Figure 3 compares the normalized TPPE spectrum of Au/DT/M-NP (the black line) with that of Au/DT/M-NP/DT (the red solid line). These data show that a shoulder appears at a high kinetic energy for the assembly of Au/DT/M-NP/DT after the ligand exchange. If one subtracts the signal of Au/DT/M-NP from that of Au/DT/M-NP/DT, the shoulder can be separated; it is shown as the red dashed line in Figure 3. It has a peak located at 1.00 ± 0.05 eV above the Fermi level.

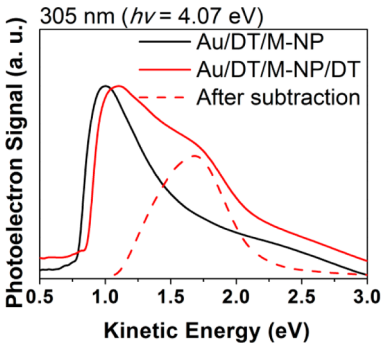

Figure 3. Comparison of the TPPE spectra for M-NP assemblies before (black solid) and after (red solid) the ligand exchange. The red-dashed line is generated by subtracting the black solid line from the red solid one.

As discussed elsewhere,[8] the kinetic energy of the photoelectrons, which arise from the LUMO in the TPPE measurement, should shift one-fold with the change of the probe photon's energy. As can be seen in Figure 4B, the separated peak shifts linearly with the probe photon's energy, and thus it is assigned to the LUMO of the M-NP. The TPPE spectra (see Figure S3) for Au/DT/S-NP/DT and Au/DT/L-NP/DT assemblies show the same general behavior, namely a shoulder arising at a high kinetic energy that shifts linearly with the probe photon energy, see panels A and C of Figure 4. From these data, the LUMO energies are determined to be 1.07 ± 0.05 eV for S-NPs, 1.00 ± 0.05 eV for M-NPs, and 0.88 ± 0.05 eV for L-NPs, above the Fermi level of the Au substrate. Details of this calculation are provided in the SI (see Figures S2 and S3). In Figure 4, the spectral width for the L-NPs is narrower than that of the M-NPs or S-NPs. This difference is attributed to the low kinetic energy peak in the TPPE spectra being more dominant for the L-NPs than for the S- or M-NPs. As a result it is more difficult to observe the high kinetic energy shoulder in the L-NPs TPPE spectra after the subtraction and the normalized spectrum appears narrower.

The ligand exchange with DT was found to increase the exciton lifetime of the NPs as well as the lifetime of trapped electrons in the LUMO of the NP. This fact was demonstrated by comparing surface photoluminescence (PL) spectra for the assemblies of Au/DT/NP and Au/DT/NP/DT. While a significant photoluminescence signal from the assemblies of Au/DT/NP/DT could be obtained (see Figure S4, SI), no measurable signal could be collected from the Au/DT/NP assemblies. This result supports the hypothesis that the DT ligands change the surface state distribution in a way that extends the exciton lifetime. The peak energies of the photoluminescence spectra provide a direct measure of the optical band gap of the NPs. A comparison of this optical band gap with the band gap computed from the LUMO and HOMO energy assignments is in excellent agreement (see Table 1). This latter observation substantiates the assignment of the HOMO and LUMO energies to the features in the photoemission spectra.

Despite its effect on the recombination rate and the energy distribution of surface states, the DT ligand exchange does not affect the HOMO energies of the NPs. LEPET spectra were collected for the Au/DT/NP/DT assemblies and the HOMO energies were determined to be the same as those for the Au/DT/NP assemblies. Note that the ligand exchange did change the work function for the NP assemblies from 4.2 ± 0.1 eV (for

dx.doi.org/10.1021/jp306702t | J. Phys. Chem. C 2012, 116, 17464–17472

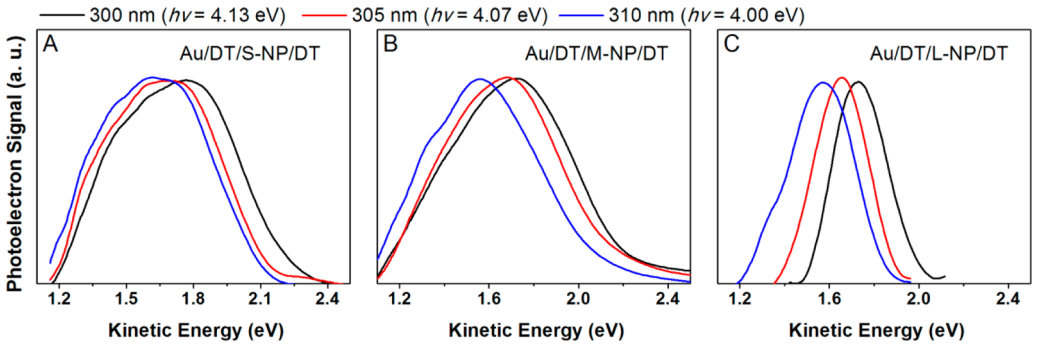

Figure 4. (A–C) TPPE spectra for the assemblies of Au/DT/S-NP/DT, Au/DT/M-NP/DT, and Au/DT/L-NP/DT; the black (4.13 eV), red (4.07 eV), and blue lines (4.00 eV) are the three different second (probe) photon energies used in the TPPE measurements (see legend).

Table 1. Band Gap of the NPs Measured by PL and PES

	bandgap (eV)	
NP	Δ_{PL}	Δ_{PES}[a]
S-NP	1.94	1.87
M-NP	1.86	1.80
L-NP	1.69	1.68

[a] Δ_{PES} has an error of ±0.1 eV.

Au/DT/NP) to 4.3 ± 0.1 eV (Au/DT/NP/DT). These data are provided in the SI (see Figure S5). This fact indicates that the HOMO level pinning is controlled by the dithiol linker between the NPs and the Au substrate. Figure 5 plots the

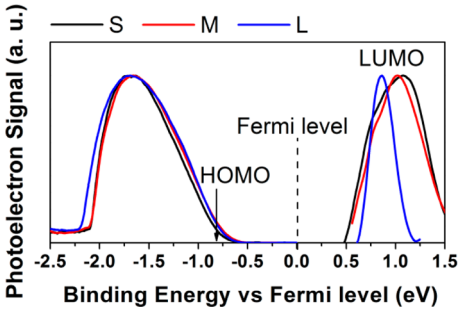

Figure 5. Plots of the LEPET and TPPE spectra together as a function of binding energy versus the Fermi level, for the three assemblies of Au/DT/NP/DT.

density of electronic states distributions obtained by PES for the three different sizes of Au/DT/NP/DT assemblies as a function of the electron binding energy. The procedure used for obtaining the density of states has been described elsewhere.[21] The zero of energy is set at the Fermi level. These data provide the density of electronic states for the NPs, and show that the HOMO is pinned at 0.80 ± 0.05 eV below the Fermi level, while the LUMO is size-dependent.

3.2. Cyclic Voltammetry. Because oxidation and reduction potentials can be directly related to the HOMO and LUMO energies of NPs,[8,22] cyclic voltammetry was used to determine the energy of the HOMO for the TDPA-capped CdTe NPs. Figure 6A shows cyclic voltammograms for the Au/DT/S-NP (black), Au/DT/M-NP (red), Au/DT/L-NP (blue), and Au/DT (SAM, dark yellow) assemblies. All of the assemblies, including the Au/DT reference system, show a weak peak near 1.0 V vs $Ag/AgNO_3$, and it is assigned to oxidation of the Au/DT. Each of the three assemblies with CdTe NPs shows two strong oxidation peaks: one at ~0.50 V vs $Ag/AgNO_3$ (O1)

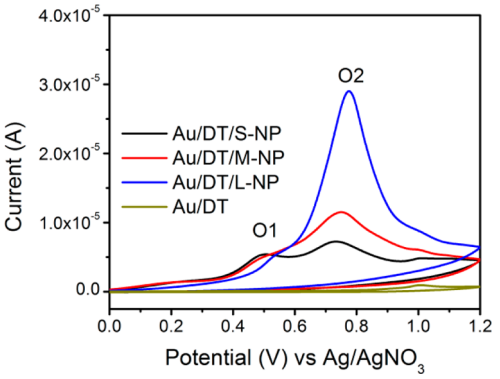

Figure 6. Voltammetry measurement in acetonitrile for the assembly of Au/DT/S-NP (black), Au/DT/M-NP (red), Au/DT/L-NP (blue), and Au/DT (SAM, dark yellow).

and one at ~0.75 V vs $Ag/AgNO_3$ (O2). The peak potentials do not shift with the size of the NP, but the magnitude of the current varies significantly with size. In fact, the signal increases as the size of the NP increases, which correlates to the increase in NP surface coverage with increasing the NP size that was observed in the SEM data (see Figure 1).

Because the strength of the peak at 0.50 V vs $Ag/AgNO_3$ (O1) varied significantly with the particular batch of NPs and the surface ligand, it is assigned to surface states of the CdTe NPs. This peak was not observed in cases where thiol-capped CdTe NPs[23] were directly synthesized with thiol ligands and used in the voltammetry studies (see Figure S6 of SI), rather than ligand exchange from TDPA-capped NPs. Ligand exchange (Scheme 2) from TDPA to DT does not remove this peak, and likely indicates that the ligand exchange may not be complete. It is important to note that the ligand exchange and different syntheses gave the same peak potential for O2. These observations are consistent with the view that thiol ligands suppress the interband surface states of the CdTe NPs. A similar observation and assignment was reported by Gaponik and co-workers.[24] Lastly, we note that the separation of 0.25 V between the peaks O1 and O2 agrees well with the energy separation (~0.30 eV) between the surface states and the valence band for CdTe NPs that was reported by Bawendi et al.[20]

The peak at 0.75 V vs $Ag/AgNO_3$ (O2) is assigned to the oxidation of the filled valence band of the NPs, and its onset oxidation potential probes the HOMO level of the NPs. Because the HOMO is the valence band maximum (or edge), it should be the first state oxidized in the voltammetry

dx.doi.org/10.1021/jp306702t | J. Phys. Chem. C 2012, 116, 17464–17472

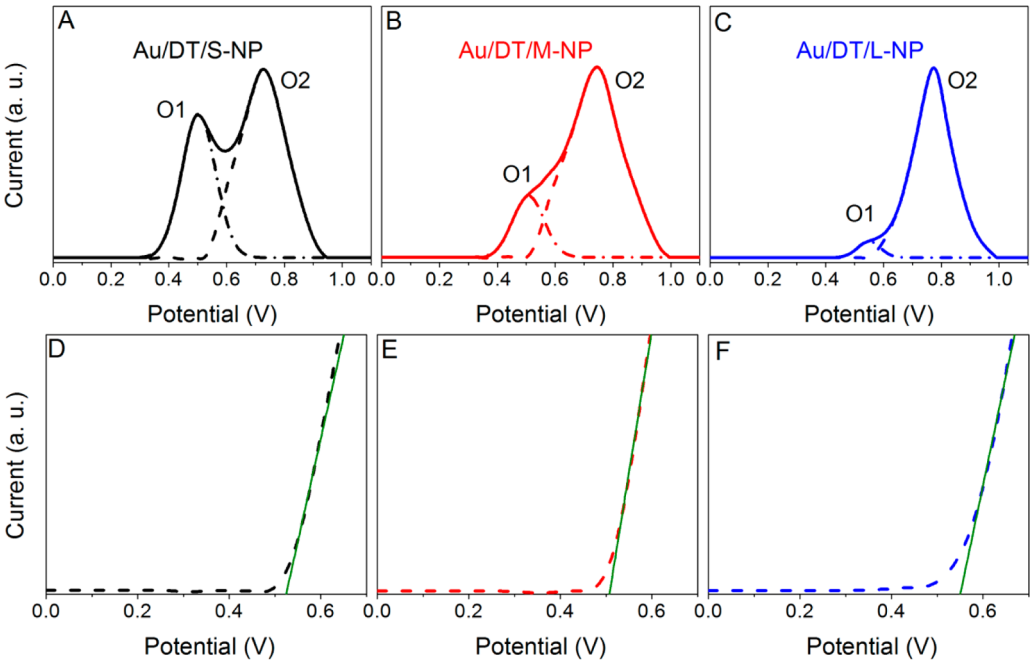

Figure 7. (A–C) Extraction of peak O2 from the oxidation wave for the assembly of Au/DT/S-NP (black), Au/DT/M-NP (red), and Au/DT/L-NP (blue), respectively. The solid curves are the oxidation wave after subtracting the simulated baseline (see Figure S7 in SI); the dashed–dotted curves are the Gaussian distribution used to fit peak O1; the dashed curves are the results after subtracting the dashed–dotted curve from the corresponding solid curve. Panels D–F show the zoomed-in view of the dash lines near the oxidation onset region, and the green lines are the linear extrapolation at the oxidation onset.

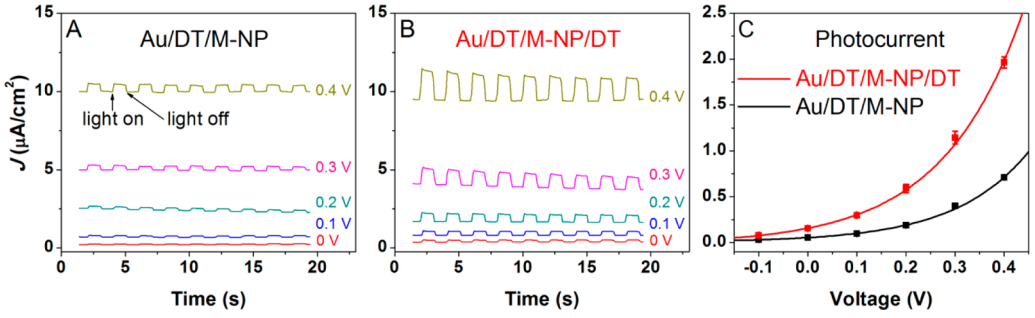

Figure 8. (A, B) Comparison of the current–time (J–t) characteristics for the assemblies of Au/DT/M-NP and Au/DT/M-NP/DT, respectively, at various voltages (3 h incubation time for the NP). (C) Photocurrent–voltage (J–V) characteristics of Au/DT/M-NP (black points) and Au/DT/M-NP/DT (red points). Lines connecting points serve a guide for the eyes. Some error bars are smaller than the symbol.

measurement, in the absence of surface states.[25−27] Because the onset potential for the peak O2 overlaps with the peak O1 from the surface states, three steps were performed to determine it. First, the peaks O1 and O2 were extracted from the measured voltammogram by subtracting a simulated baseline from the oxidation wave of Au/DT/NP (see Figure S7 in SI for details). The subtraction results are shown as the solid curves in Figure 7A–C for the three Au/DT/NP assemblies. Second, the energy distributions of the surface states O1 were assumed to be Gaussian-distributed. This assumption allowed a Gaussian distribution function (dashed-dotted line in Figure 7A–C) to be fit to the peak O1, and then subtracted from the voltammogram to isolate the peak O2 (dashed curve in Figure 7). These data reveal a sharp onset for the O2 wave (see Figure 7D–F), which allowed the onset potential to be determined by a linear extrapolation (green lines) to zero current. The results in Figure 7D–F show that the oxidation for the three sizes of the NPs all start at about 0.5 ± 0.1 V; thus, their HOMO is pinned at about 0.5 V vs $Ag/AgNO_3$. By taking the absolute electrode potential of $Ag/AgNO_3$ in acetonitrile to be 4.7 eV,[28] the onset oxidation potential (E_{ox}) can be converted to the HOMO energy versus vacuum (E_{HOMO}) by way of the equation: $E_{HOMO} = -[E_{ox} + 4.7]$ eV. The HOMO pinning energy, relative to the vacuum level, that is derived from the voltammetry measurement is −5.2 ± 0.1 eV, and it is in good agreement with that measured from PES (−5.0 ± 0.1 eV). The ~0.1 eV difference may be caused by solvation and other interfacial effects that are present in the voltammetry measurement, but not in the PES measurement.

Attempts to measure the NP reduction potential proved challenging and somewhat irreproducible. Several other groups have also reported the absence of reduction signal in their voltammetry experiments for CdSe NPs.[29,30] We also note that the oxidation of the NP is very irreversible even when a hole scavenger, such as triethanolamine, is present in the solution.

3.3. Photocurrent Studies. If DT ligand exchange reduces the charge recombination rates in the NPs, then it should enhance the charge transfer through NP films. The impact of

dx.doi.org/10.1021/jp306702t | J. Phys. Chem. C 2012, 116, 17464–17472

the DT ligand exchange on the charge carrier transport was assessed by photocurrent measurements of the monolayer assemblies in an electrochemical cell. Panels A and B of Figure 8 show the current density-time ($J-t$) characteristics for the Au/DT/M-NP and Au/DT/M-NP/DT assemblies. It is apparent that the photocurrent produced by Au/DT/M-NP/DT is much higher than that of Au/DT/M-NP under the same bias voltage. In Figure 8C, the light-off current (dark current) is subtracted from each corresponding $J-t$ characteristic in A and B of Figure 8 to obtain the photocurrent density−voltage ($J-V$) characteristic. These data show that the photocurrent for the Au/DT/M-NP/DT assemblies is at least four times higher than that for the corresponding Au/DT/M-NP assemblies. Similar results were reproduced for different NP coverages on the Au electrode (see Figure S8). This observation further supports the conclusion that the DT molecules extend the NP exciton lifetime, and therefore improve the photoconductivity of the NP film.

A simple Schottky barrier (diode) model was able to fit the photocurrent data (see Figure S9, SI) for the assemblies of Au/DT/M-NP and Au/DT/M-NP/DT. The Schottky barrier heights ($\Delta\phi$) that were extracted from the fitting (see in Table S1, SI) indicate that the ligand exchange from TDPA to DT slightly reduces the Schottky barrier height for electron transfer from the NP to the Au electrode.

4. DISCUSSION

4.1. Why Is the HOMO Pinned? When a semiconductor and a metal substrate are brought into contact, charge rearranges until the Fermi levels of the semiconductor and the metal coincide. This charge rearrangement creates an electrical field across the interface.[8] For realistic systems with a high density of surface states this charge rearrangement can be dominated by changes in charge population of the surface states over a narrow band of energies. Thiol-coated gold electrodes have a high density of surface states at energies of about 1.2−1.6 eV below the Fermi level.[8,31] We postulate that these surface states couple strongly with the nanoparticle states and set the final energy position for the HOMO with respect to the Au Fermi level. A quantitative model for this effect should account for the electric field that is generated between the NP and the Au, and it should account for the electronic coupling between the NP and the Au, which can affect the NPs electronic confinement. If the HOMO couples more strongly to the substrate than the LUMO, then the LUMO states of the NP remain more localized. As Brus[32] has pointed out, this implies an increase (decrease) of the effective mass of the hole (electrons) in the HOMO (LUMO). Thus, the effective mass of the electron is smaller than what one might expect from comparing to that in the unbound NPs.

4.2. Why Onset Potential? Because the semiconductor NP assemblies do not display reversible redox waves, the averaging of oxidation and reduction waves to determine the formal potential of the NP cannot be used. The often asymmetric voltammograms of the NPs indicate that their redox reaction is highly irreversible. In addition, it has been noted by Bard and co-workers[25] that the oxidation of the NPs can be a multicharge transfer process, in which the second charge injected into the NPs from the electrode must overcome the "Coulombic blockade" from the first charge injected. Given these constraints, the onset oxidation potential provides a reasonable and clear method for estimating the energy required for the first charge injected into the HOMO level of the NPs in the ground state. Another important reason for using the onset potential for the HOMO is the poor electrochemical stability of the NPs. Several groups have reported that the electrochemical charge injected into the NPs subsequently undergoes a fast coupled chemical reaction (an EC reaction) related to NP decomposition,[22,33] such as, $CdTe \rightarrow Cd^{2+} + Te^{0} + 2e^{-}$. This fact can be visualized by comparing the LEPET energy distribution with the voltammogram for the CdTe NPs used in this work, as shown in Figure 9. It is apparent that these two distributions do not agree with each other except near the onset region. Comparing the width of these two distributions suggests that the voltammetry does not reveal the full distribution of the electronic states in the NPs. For these reasons, the onset oxidation potential was used to quantify the HOMO energy of the NPs.

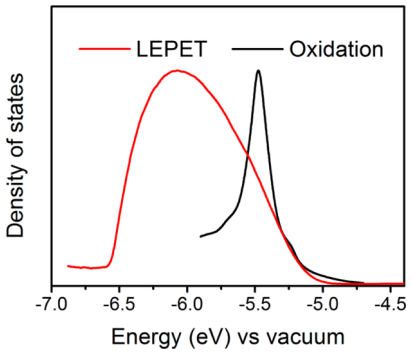

Figure 9. Comparison of approximated density of electronic states obtained from LEPET (red line) and the voltammetry (black line) measurements for the large CdTe NPs used in this work. Using the data for the medium/small CdTe NPs or the CdSe NPs will give similar results.

In our earlier report on CdSe NPs,[8] the peak oxidation potential was used to calculate the HOMO energy, and this choice created a difference of ~0.3 eV between the PES and voltammetry results. However, if the onset oxidation potential is used rather than the peak potential, the agreement between the PES and voltammetry measurements of the HOMO energy is much better. Figure 10 shows that the HOMO pinning level measured from the onset oxidation potentials (black open

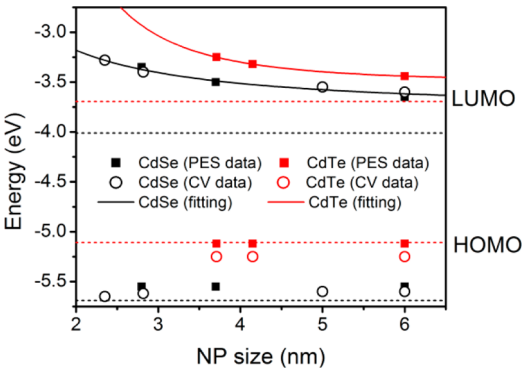

Figure 10. Comparison of the energetics (HOMO/LUMO) for the CdSe (data in black) and CdTe NPs (data in red). The filled squares are results from the PES measurements, and the open circles are ones from the voltammetry. The dash lines are the bandedge energies in the bulk CdSe and CdTe semiconductors; and the solid lines are the fitting to the LUMO energies.

circles) is only about 0.1 eV lower than that from the PES (black filled squares) for the CdSe NPs. Figure 10 also compares the band edge energies (HOMO/LUMO) for CdSe (data in black) and CdTe (data in red) NPs. These data demonstrate the good agreement between the PES (filled squares) and voltammetry (open circles) measurements. These data reveal that the HOMO energies of the immobilized CdSe and CdTe NPs are independent of the NP size (for sizes greater than 2.8 nm and less than 6 nm), while the LUMO energies shift systematically with the NP size over this same size range. The solid curves are fits of the data to a power law (see SI), which can be helpful for predicting the LUMO/HOMO energies and band gaps for the CdSe and CdTe NPs.

The data in Figure 10 reveal that CdSe NPs and CdTe NPs can be used to form a type-2 heterojunction. This fact is in agreement with earlier reports.[2,3,14,34] While the results in Figure 10 agree with the photoemission data in reference 14 for CdSe NPs, we note that they indicate that the HOMO (−5.55 eV) for the CdSe NPs is higher than CdSe bulk valence band edge (−5.7 eV). In addition, the band edge positions for the CdSe and CdTe NPs do not show a similar behavior with respect to their bulk energetics. This feature of the observations poses a challenge for theoretical models and calculations.

5. CONCLUSION

This work used photoelectron spectroscopy and electrochemistry to measure the electronic states of CdTe NP assemblies on Au electrodes. The measurements revealed that the HOMO energy of the NPs is fixed, whereas the LUMO energy of the NPs changes with NP size, over a range from 3.7 to 6.0 nm. The electrochemical and photoelectron determinations of the HOMO energies were found to agree with one another to within ∼100 mV. Two photon PES measurements and photocurrent measurements were used to show that thiol capping ligands reduce the recombination rate of charge carriers in CdTe NPs.

■ ASSOCIATED CONTENT

Supporting Information

Figure S1 shows the LEPET spectra for the NPs with different surface coverage on the Au substrate. Figure S2 and Figure S3 compare the TPPE spectra for the assemblies of Au/DT/NPs and Au/DT/NPs/DT measured at three different wavelengths. Figure S4 presents the photoluminescence spectra for the assemblies of Au/DT/NPs/DT. Figure S5 compares the LEPET spectra for the assemblies of Au/DT/NPs and Au/DT/NPs/DT. Figure S6 shows the voltammetry results for the three sizes of CdTe NPs that were originally synthesized in the aqueous phase with a water-soluble thiol ligand (3-mercaptopropionic acid, MPA). Figure S7 shows the simulated baseline for the NP oxidation wave of the voltammograms shown in Figure 6. Figure S8 compares the photocurrent−voltage characteristics of Au/DT/M-NP and Au/DT/M-NP/DT with different NP incubation times. Figure S9 shows that a simple Schottky barrier (diode) model was able to fit the photocurrent data for the assemblies of Au/DT/M-NP and Au/DT/M-NP/DT. Table S1 lists the fitting parameters and the extracted Schottky barrier height in Figure S9. Finally, the equations used to fit the LUMO energy of the CdTe and CdSe NPs are listed at the end of the Supporting Information. This material is available free of charge via the Internet at http://pubs.acs.org.

■ AUTHOR INFORMATION

Corresponding Author

*ron.naaman@weizmann.ac.il (R.N.); dave@pitt.edu (D.H.W.).

Author Contributions

⊥These authors contributed equally to this work.

Notes

The authors declare no competing financial interest.

■ ACKNOWLEDGMENTS

This work was supported by the U.S. Department of Energy (Grant No. ER46430).

■ REFERENCES

(1) Anikeeva, P. O.; Halpert, J. E.; Bawendi, M. G.; Bulovic, V. *Nano Lett.* **2007**, *7*, 2196.
(2) Gur, I.; Fromer, N. A.; Geier, M. L.; Alivisatos, A. P. *Science* **2005**, *310*, 462.
(3) Wang, Y.; Wang, L.; Waldeck, D. H. *J. Phys. Chem. C* **2011**, *115*, 18136.
(4) Huynh, W. U.; Dittmer, J. J.; Alivisatos, A. P. *Science* **2002**, *295*, 2425.
(5) Burda, C.; Chen, X. B.; Narayanan, R.; El-Sayed, M. A. *Chem. Rev.* **2005**, *105*, 1025.
(6) Ruhle, S.; Shalom, M.; Zaban, A. *ChemPhysChem* **2010**, *11*, 2290.
(7) Luther, J. M.; Law, M.; Beard, M. C.; Song, Q.; Reese, M. O.; Ellingson, R. J.; Nozik, A. J. *Nano Lett.* **2008**, *8*, 3488.
(8) Markus, T. Z.; Wu, M.; Wang, L.; Waldeck, D. H.; Oron, D.; Naaman, R. *J. Phys. Chem. C* **2009**, *113*, 14200.
(9) Xie, Z. T.; Markus, T. Z.; Gotesman, G.; Deutsch, Z.; Oron, D.; Naaman, R. *ACS Nano* **2011**, *5*, 863.
(10) Carlson, B.; Leschkies, K.; Aydil, E. S.; Zhu, X. Y. *J. Phys. Chem. C* **2008**, *112*, 8419.
(11) Timp, B. A.; Zhu, X. Y. *Surf. Sci.* **2010**, *604*, 1335.
(12) Sze, S. M.; Ng K. K. *Physics of Semiconductor Devices*, 3rd ed.; Wiley: New York, 2007.
(13) Haram, S. K.; Kshirsagar, A.; Gujarathi, Y. D.; Ingole, P. P.; Nene, O. A.; Markad, G. B.; Nanavati, S. P. *J. Phys. Chem. C* **2011**, *115*, 6243.
(14) Jasieniak, J.; Califano, M.; Watkins, S. E. *ACS Nano* **2011**, *5*, 5888.
(15) Soreni-Harari, M.; Yaacobi-Gross, N.; Steiner, D.; Aharoni, A.; Banin, U.; Millo, O.; Tessler, N. *Nano Lett.* **2008**, *8*, 678.
(16) Yu, W. W.; Wang, Y. A.; Peng, X. G. *Chem. Mater.* **2003**, *15*, 4300.
(17) Yu, W. W.; Qu, L. H.; Guo, W. Z.; Peng, X. G. *Chem. Mater.* **2003**, *15*, 2854.
(18) Naaman, R.; Sanche, L. *Chem. Rev.* **2007**, *107*, 1553.
(19) Wuister, S. F.; Donega, C. D.; Meijerink, A. *J. Phys. Chem. B* **2004**, *108*, 17393.
(20) Geyer, S.; Porter, V. J.; Halpert, J. E.; Mentzel, T. S.; Kastner, M. A.; Bawendi, M. G. *Phys. Rev. B* **2010**, *82*, 155201.
(21) Markus, T. Z.; Daube, S. S.; Naaman, R. *J. Phys. Chem. B* **2010**, *114*, 13897.
(22) Haram, S. K.; Quinn, B. M.; Bard, A. J. *J. Am. Chem. Soc.* **2001**, *123*, 8860.
(23) Rogach, A. L.; Franzl, T.; Klar, T. A.; Feldmann, J.; Gaponik, N.; Lesnyak, V.; Shavel, A.; Eychmuller, A.; Rakovich, Y. P.; Donegan, J. F. *J. Phys. Chem. C* **2007**, *111*, 14628.
(24) Poznyak, S. K.; Osipovich, N. P.; Shavel, A.; Talapin, D. V.; Gao, M. Y.; Eychmuller, A.; Gaponik, N. *J. Phys. Chem. B* **2005**, *109*, 1094.
(25) Ding, Z. F.; Quinn, B. M.; Haram, S. K.; Pell, L. E.; Korgel, B. A.; Bard, A. J. *Science* **2002**, *296*, 1293.
(26) Zhong, H. Z.; Lo, S. S.; Mirkovic, T.; Li, Y. C.; Ding, Y. Q.; Li, Y. F.; Scholes, G. D. *ACS Nano* **2011**, *4*, 5253.
(27) Li, Y. C.; Zhong, H. Z.; Li, R.; Zhou, Y.; Yang, C. H.; Li, Y. F. *Adv. Funct. Mater.* **2006**, *16*, 1705.

(28) By using the work function of ferrocene (4.8 eV) and the redox potential (0.1 V) of Ag/$AgNO_3$ vs ferrocene, the work function of Ag/$AgNO_3$ is calculated to be 4.7 eV.
(29) Myung, N.; Ding, Z. F.; Bard, A. J. *Nano Lett.* **2002**, *2*, 1315.
(30) Zotti, G.; Vercelli, B.; Berlin, A.; Chin, P. T. K.; Giovanella, U. *Chem. Mater.* **2009**, *21*, 2258.
(31) Alloway, D. M.; Hofmann, M.; Smith, D. L.; Gruhn, N. E.; Graham, A. L.; Colorado, R.; Wysocki, V. H.; Lee, T. R.; Lee, P. A.; Armstrong, N. R. *J. Phys. Chem. B* **2003**, *107*, 11690.
(32) Brus, L. E. *J. Chem. Phys.* **1984**, *80*, 4403.
(33) Chen, S. W.; Truax, L. A.; Sommers, J. M. *Chem. Mater.* **2000**, *12*, 3864.
(34) Wu, M. Y.; Mukherjee, P.; Lamont, D. N.; Waldeck, D. H. *J. Phys. Chem. C* **2010**, *114*, 5751.